Applied Surface Science 292 (2014) 128–136

Contents lists available at ScienceDirect

Applied Surface Science

journal homepage: www.elsevier.com/locate/apsusc

Controlling formation of gold nanoparticles generated *in situ* at a polymeric surface

Christopher J. Clukay[a], Christopher N. Grabill[a], Michelle A. Hettinger[a], Aniruddha Dutta[b,c], Daniel J. Freppon[a], Anthony Robledo[b], Helge Heinrich[b,c], Aniket Bhattacharya[b], Stephen M. Kuebler[a,b,d,*]

[a] Department of Chemistry, University of Central Florida, Orlando, FL 32816, USA
[b] Department of Physics, University of Central Florida, Orlando, FL 32816, USA
[c] Advanced Materials Processing and Analysis Center, Orlando, FL 32816, USA
[d] CREOL, The College of Optics and Photonics, University of Central Florida, Orlando, FL 32816, USA

ARTICLE INFO

Article history:
Received 13 June 2013
Received in revised form
28 September 2013
Accepted 19 November 2013
Available online 26 November 2013

Keywords:
Gold nanoparticle
Polymer surface
SU-8
Plasmonics
Catalysis

ABSTRACT

This work shows that *in situ* reduction of metal ions bound at a polymer surface can form nanoparticles within the polymer matrix as well as at the interface, and the size and distribution of nanoparticles between the interface and subsurface depends upon the choice of reagents and reaction conditions. Tetrachloroaurate ions were bound to cross-linked SU-8 films that were functionalized using a variety of multi-functional amines, then reduced using one of several reagents. Reduction using sodium borohydride or sodium citrate generates bands of interspersed gold nanoparticles as much as 40 nm deep within the polymer, indicating that both the Au ions and the reducing agent can penetrate the surface enabling formation of nanoparticles within the polymer matrix. Nanoparticle formation can be confined nearer to the polymer interface by reducing with hydroquinone, or by processing the polymer film in aqueous media using high molecular-weight multifunctional amines that confine the gold ions at the interface.

1. Introduction

Gold nanoparticles (Au NPs) and clusters or arrays of surface-bound Au NPs have a wide variety of applications, including nanofabrication, optical devices, and catalysis [1–11]. Au NPs and nanoparticle-aggregates are effective for enhancing signal via surface plasmon resonance in various spectroscopic and sensing methods [12,13]. Metal nanoparticles (NPs) are used as nucleation sites in electroless metallization, which is a promising approach for creating metallized micro-electromechanical structures (MEMS) and optical MEMS devices [7,14–18]. Such applications frequently involve Au–NP functionalization of a polymeric surface or structure. As such, NP synthesis and surface functionalization continue to be active areas of research that impact many established and emerging technologies.

The common approach for functionalizing surfaces with NPs involves first synthesizing colloidal particles in solution and subsequently binding them to the surface of interest, using the Turkevich method [7,8,12,18–21] or sodium borohydride ($NaBH_4$) reduction [13,20,22–25]. In contrast, *in-situ* reduction of gold ions adsorbed onto a surface is an alternative means for generating Au NP-functionalized surfaces and devices [1,2,26–30]. This approach offers some advantages, including the possibility for generating smaller particles, stabilization of the NPs through surface attachment, and decreased aggregation due to immobilization on the surface [1,30,31]. Additionally, surface-bound NPs can be readily isolated from the synthesis medium or further derivitized by simple physical transfer of the supporting substrate. There are several pioneering reports of *in-situ* synthesis of Au NPs at polymeric surfaces [1–3,28,30–33]. Yet in comparison to the conventional approach of separately synthesizing NPs then binding them to a surface, *in-situ* synthesis of Au NPs at polymeric surface remains far less explored.

In this work we show how the choice of gold-ion surface-linker and reducing agent affects *in-situ* formation of Au NPs at the surface of a polymer known as "SU-8". SU-8 is a cross-linkable epoxide which is increasingly employed for patterning micro- and nano-scale surfaces and creating functional devices [25,34–36]. The key findings of this work are (1) NPs formed by *in-situ* reduction do

* Corresponding author. Tel.: +1 407 823 3720; fax: +1 407 823 2252.
E-mail addresses: cclukay@knights.ucf.edu (C.J. Clukay), chem_chris@knights.ucf.edu (C.N. Grabill), drew41989@knights.ucf.edu (M.A. Hettinger), aniruddha@knights.ucf.edu (A. Dutta), dfreppon@knights.ucf.edu (D.J. Freppon), anthonyrobledo@gmail.com (A. Robledo), helge.heinrich@ucf.edu (H. Heinrich), aniket@physics.ucf.edu (A. Bhattacharya), kuebler@ucf.edu, smkuebler@gmail.com (S.M. Kuebler).

0169-4332/$ – see front matter © 2013 Elsevier B.V. All rights reserved.
http://dx.doi.org/10.1016/j.apsusc.2013.11.099

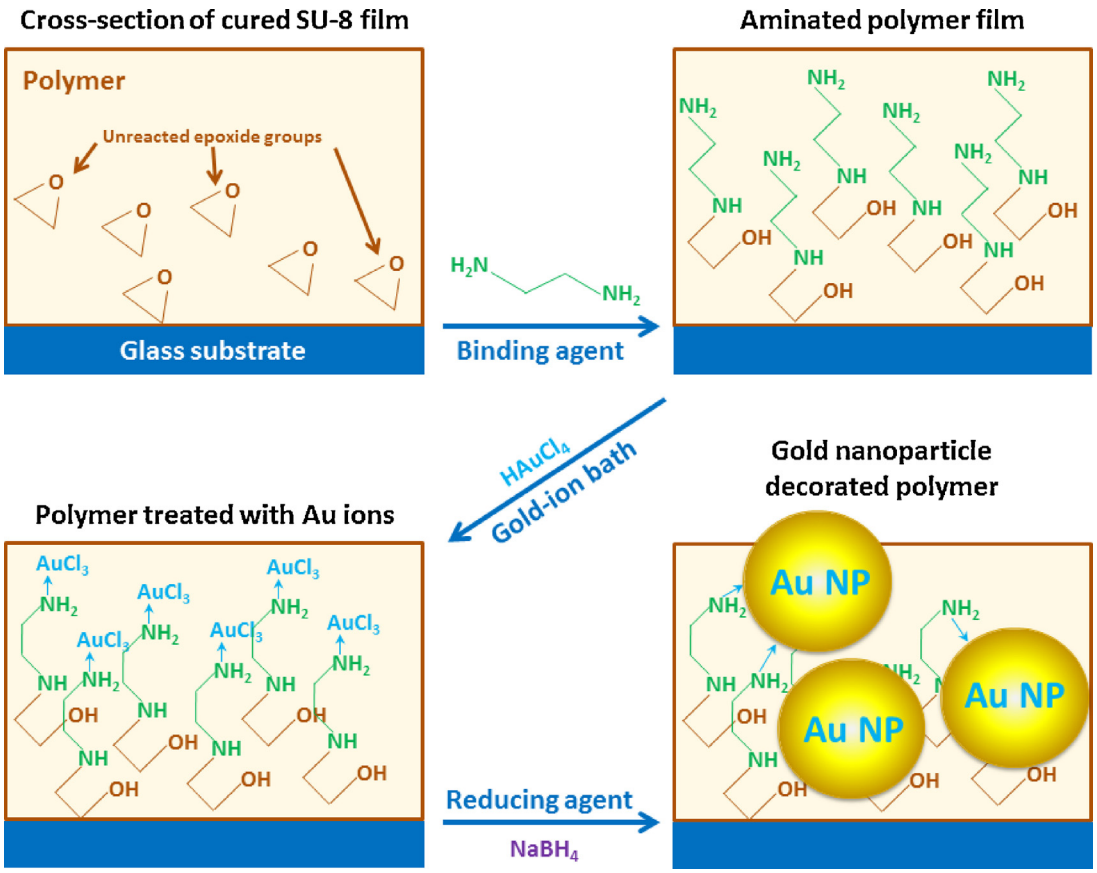

Fig. 1. Illustration of the process used to functionalize the surface of cross-linked polymer SU-8 with Au NPs. Each panel represents a cross-section of the polymer film through the surface. The scheme is illustrated for the case in which Au ions are bound to the polymer film surface using ED then reduced by $NaBH_4$, and only one possible mode of Au-amine interaction is represented.

not reside exclusively at the liquid-polymer interface; (2) varying the reducing agent can affect both the size of the NPs and their location relative to the interface; and (3) formation of Au NPs can be confined to the liquid-polymer interface by judicious choice of the amine binding agent and how it is processed.

2. Material and methods

2.1. Preparation of gold nanoparticle functionalized films

All commercial materials were reagent grade and used as received unless otherwise indicated. Deionized water (18 MΩ) was used to rinse all samples and prepare all aqueous solutions. The process of polymer surface modification is illustrated in Fig. 1, for the case of the binding agent ethylenediamine (ED) and reducing agent $NaBH_4$. All reactions and solution preparation were carried out under ambient conditions unless otherwise stated.

Square glass coverslips (25 mm, no. 1 thickness) served as substrates and were cleaned by immersion in an aqueous 1 M KOH bath (Aldrich and Fisher, technical grade) for 1 h followed by drying in an oven at 100 °C for 20 min. Cross-linked SU-8 films were prepared by spin coating the epoxide resin (SU-8 2035, Microchem) onto cleaned substrates. Solvent was removed from the resin film by baking the samples on a hotplate. The samples were placed on a hotplate at room temperature, heated over a period of one minute to 95 °C, held at this temperature for 9 min, then the hot plate was switched off and the samples were allowed to cool to room temperature (*circa* 10 min). The resin films were subsequently irradiated for 2 min through a long-pass filter (Omega Optical, PL-360LP, 360-nm cut off) with a broad-band UV lamp (Loctite ZETA 7411-5, 400 W metal halide source, 315–400 nm) then baked to activate cross-linking using the same conditions as the pre-exposure bake.

Cross-linked polymer surfaces were activated toward binding Au cations by covalently attaching one of several multifunctional primary amines (Fig. 2). Functionalization with ED was achieved by immersing the cross-linked polymer film into a 20% (v/v) of ED (Alfa Aesar, CAS no. 107-15-3) in ethanol for 1 h [37,38]. Functionalization with tetraethylenepentamine (TEPA, CAS no. 112-57-2) and *N*-aminoethylpiperazine (AEP, CAS no. 140-31-8) were similarly achieved by immersing samples in 20% (v/v) aqueous solutions of the amines for 1 h. Following amination, all samples were rinsed with copious water and allowed to dry by standing in air.

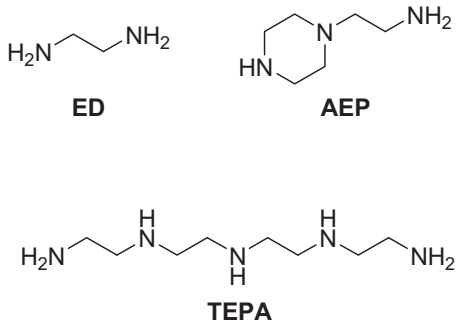

Fig. 2. Multi-functional amines used to bind gold cations to the surface of cross-linked SU-8.

Au NP functionalized polymer surfaces were prepared by binding Au cations to aminated SU-8 films and then immediately treating with a reducing agent. The conditions selected for the reduction step were chosen to be as similar as possible to those most commonly employed for synthesis of Au NPs in solution. Amine-functionalized polymer films were placed in aqueous 5.3×10^{-4} M $HAuCl_4$ (Acros, CAS no. 16961-25-4) for 30 min at room temperature, rinsed with copious water, then immersed into a reduction bath for 60 s consisting of aqueous 0.1 M $NaBH_4$ (Fisher, CAS no. 16940-66-2) [7,20,22]. Reduction using citrate was accomplished, similar to the method of Khalid et al. [1], by immersing samples for 8 h in aqueous 1% (w/v) sodium citrate ($Na_3C_6H_5O_7$, Fisher, CAS no. 6132-04-3). Reduction with hydroquinone was achieved by immersing samples in aqueous 0.1 M hydroquinone (Acros, HOC_6H_4OH, CAS no. 123-31-9) for 1 h [39]. After reduction, samples were rinsed with copious water and allowed to dry by standing in air.

2.2. Analysis by transmission electron microscopy

Samples for plan-view imaging were prepared by scraping a thin section from the surface of the polymer film (*circa* 100-nm thick) and transferring it to a copper grid for imaging. For cross-sectional imaging, samples were first coated with carbon for 30 s in a vacuum evaporator (Jeol JEE 4X), to increase the contrast of the transmission electron microscopy (TEM) image and enable easy identification of Au NPs on or near the polymer surface. Each sample was then coated with Au–Pd using a sputter coater (Emitech K550) equipped with a 60-mm diameter and 0.1-mm thick magnetron target assembly. This instrument deposits metal as fine grains, without the need to cool the specimen. Sample cross-sections were prepared using a TEM focused ion beam (FIB) instrument (FEI 200) equipped with a 30 kV gallium liquid metal ion source. A 1-μm thick layer of Pt was deposited onto a rectangular strip 20 μm × 1 μm to mask the region intended for the cross-section. Through Ga-ion milling, a sample cross-section having 20-μm width, 0.15-μm thickness, and 4-μm height was obtained. A micromanipulator was then used to lift out the milled cross-section and transfer it onto a carbon-coated copper grid for TEM imaging.

A Tecnai F30 operating at 300 kV was used to image samples in both plan view and cross section. Micrographs obtained from the instrument had a point-to-point image resolution of 0.2 nm. Both low magnification and high-resolution images were acquired. Energy dispersive spectroscopy (EDS) and energy filtered TEM were used to confirm that particles imaged were in fact gold. High-angle annular dark-field (HAADF) imaging in the scanning transmission electron microscopy (STEM) mode was used to analyze particle sizes. Sample cross sections were progressively tilted during imaging to obtain accurate minimum widths for bands of Au NPs observed at or near the polymer surface.

Particle heights were measured using calibrated HAADF–STEM pixel intensities. The projected particle area was obtained from perimeter fitting, and the corresponding volume was estimated by integrating the HAADF–STEM pixel-intensity over that area. A total of 150 particles were analyzed to obtain the distribution of particle radii, heights, and volumes, and their corresponding means for a given sample. For comparison, the mean volume-from-height was calculated using the equation for the volume of an ellipsoid, the mean particle height, and the mean lateral radii. A given size dispersion was treated as a normal distribution, and the width of the distribution is reported as a relative standard deviation (RSD) of the parameter.

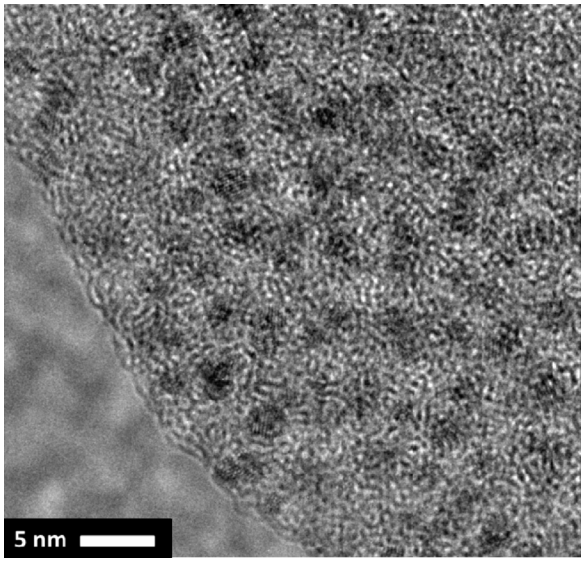

Fig. 3. Bright-field plan-view TEM micrograph of Au NPs generated *in situ* by binding gold ions at the SU-8 polymer surface with ED then reducing with $NaBH_4$.

2.3. Analysis by X-ray photoelectron spectroscopy

Elemental composition of Au–NP decorated surfaces was determined from X-ray photoelectron spectroscopy (XPS, Physical Electronics 5400 ESCA) using an unmonochromated Mg source at 15 kV potential and constant power of 300 W with a pass energy of 35.75 eV. Carbon due to SU-8 was used as an internal reference [40] to correct for absolute peak shifts that result from surface charging [41]. Special care was taken to minimize exposure of the samples to the X-ray source prior to the start of an analysis, and sample positioning prior to the start resulted in no more than 30 s of unwanted exposure. Spectra were collected in multiple scans as a function of X-ray exposure time, to obtain a time-dependent analysis of how X-ray exposure affected the oxidation state of surface-bound gold. The spectra were corrected for linear baseline shift and fit using a series of Gaussian–Lorentz curves (Augerscan Ver. 3.22, RBD Instruments). For peaks due to Au, each oxidation state was represented by a pair of curves separated by 3.67 eV and having curve-areas locked to the 3:4 ratio expected due to spin-orbit splitting of the $4f_{5/2}$ and $4f_{7/2}$ levels, respectively [42]. All curve fits were performed using least squares minimization, and each gave a mean-squared error below 2.0 counts.

2.4. Analysis by atomic force microscopy

Surface topography of the Au–NP-decorated films was measured after each stage of their preparation using tapping-mode atomic force microscopy (AFM, Veeco Dimension 3100 Combination SPM). The measurements were performed using AppNano ACT silicon tips (~300 kHz resonance frequency), 1-Hz scan rates, and 256 samples per line. Each AFM image was scaled to the maximum height-difference. The root-mean-squared error in the surface-height measurements is on the order of 0.05 nm.

3. Results and discussion

3.1. Nanoparticle characteristics and surface distribution

Fig. 3 shows a plan-view bright-field TEM image of Au NPs generated by reduction of gold ions bound at the polymer surface using ED then reduced using $NaBH_4$. It is important to note that this imaging mode shows features in *projection*, so the nanoparticles visible

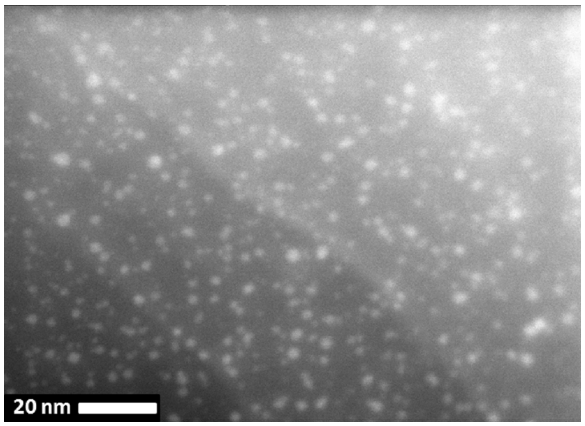

Fig. 4. HAADF–STEM image of Au NPs generated *in situ* by binding gold ions at the SU-8 polymer surface with ED then reducing with $NaBH_4$.

may be bound at the interface or *within* the polymer film. Elemental analysis line scans obtained during plan-view imaging, as well as cross-sectional imaging discussed below, consistently indicate the round high-contrast features are gold. Au NPs form on or near the surface, randomly distributed, with almost no aggregation and no long range order. Although minor faceting can be observed for select particles, as a whole they appear to be agglomerations of gold atoms, which also lack a definite periodicity. However, by the very nature of the present work, the Au NPs are always viewed against a background of amorphous polymer that significantly reduces contrast relative to that achievable in conventional TEM imaging, where samples are supported on a thin grid. Consequently, the Au NPs may in fact have a definite atomic periodicity that is simply not visible for most nanoparticles.

HAADF–STEM images like that shown in Fig. 4 were analyzed using integrated pixel intensity to obtain estimates for the shape and size of particles formed by *in situ* reduction. Comparison of similar plan-view (as well as cross-sectional images, see below) indicate that the dispersion in particle size and spatial homogeneity seen in Figs. 3 and 4 is typical for samples produced by this process. Based on the particle-size analysis, Au NPs formed by $NaBH_4$ reduction are best described as oblate spheroids. Integrated pixel intensity measurements yielded an average volume of 8.5 nm^3, with a standard deviation (width of particle–volume distribution) of 4.8 nm^3, or an RSD of 60%. This wide distribution arises from large variation observed in both the lateral and vertical radii of the particles. The measured particle heights (normal to the surface) average to 1.8 nm with an RSD of 40%. The average lateral radius is 1.4 nm with a RSD of 21%. From these values, one can calculate an average particle volume-from-height of 7.3 nm^3, which agrees well with the value obtained from integrated pixel intensities. These particle sizes are comparable to that obtained by synthesis of Au NPs in solution [20,22] and other reports of Au NP generated *in situ* using $NaBH_4$ [27,28,30].

3.2. Controlling nanoparticle size and distribution relative to the interface

We examined how the choice of reducing agent used to prepare the Au NPs affects their size and resulting distribution laterally at (or near) the polymer surface and vertically with respect to the interface. In addition to $NaBH_4$, sodium citrate and hydroquinone were selected for this portion of the study, as they are widely used for metal cation reduction and preparing Au NPs in solution [12,19,20,22,23,30,43]. From the TEM cross-sectional images of Fig. 5, it is immediately obvious that the size of the Au NPs varies substantially, depending on which of the reducing agents is utilized. $NaBH_4$ generates Au NPs in a band that spans from the interface into the polymer film to a depth of approximately 20 nm. These particles are mostly small (radius less than 5 nm). Citrate-generated Au NPs appear to form in two distinct bands of significantly different sizes, and both are larger than those generated with $NaBH_4$. The first band consists of large Au NPs (radius >5 nm) located at the polymer interface. The second band consists of small Au NPs, comparable in size to those generated by $NaBH_4$, that are spread across a band approximately 40 nm wide and centered 20 nm below the polymer interface. Reduction with hydroquinone appears to generate only the larger Au NPs, having a diameter of 10–20 nm, consistent with reports of synthesis of Au NPs in solution using hydroquinone [30]. Interestingly, Au NPs generated with hydroquinone reside in a *single* band located at or within 10 nm of the polymer interface. Repeated experiments using each reducing agent showed that the observations described above were highly reproducible.

The difference in size of particles generated *at* versus *below* the interface may result from the difference in species mobility within the polymer matrix versus at the interface, as well as a difference in strength of the reducing agents. Studies in solution show that strong reducing agents promote formation of small Au NPs, because rapid reduction favors nucleation over diffusion limited growth of larger particles [44–46]. Values for the standard reduction potentials of $NaBH_4$, hydroquinone, and citrate are −1.37 V [47], +0.699 V [48], and +1.2 V,[1] respectively, referenced to the normal hydrogen electrode. Consistent with this, the smallest Au NPs observed in this work are generated by $NaBH_4$, the strongest reducing agent used.

The TEM cross-sections suggest both $NaBH_4$ and sodium citrate are capable of diffusing into the polymer matrix sufficient to generate Au NPs below the surface. In contrast, hydroquinone generates Au NPs only at or near the polymer interface. Relative to $NaBH_4$ and sodium citrate, the greater rigidity and steric bulk of hydroquinone may reduce its ability to diffuse into the polymer matrix, so that Au NPs are only generated by hydroquinone at the interface.

The outcome of reduction by citrate is intermediate between that observed with $NaBH_4$ and hydroquinone, in that small Au NPs are generated within the polymer matrix, yet large Au NPs are produced at the interface as well. Au ions located at the interface are expected to have higher mobility than those within the matrix, so particle growth should be more favorable at the interface, especially with weaker reducing agents. Consequently, Au NPs generated at the interface with both sodium citrate and hydroquinone are much larger than those generated within the polymer matrix. Comparing the size of Au NPs produced within the polymer matrix reveals they are larger when produced with citrate than with $NaBH_4$, consistent with the former being the weaker reducing agent. Interestingly, both the large and small Au NPs observed for *in-situ* reduction by citrate are within the range of sizes observed when prepared in solution (5–147 nm), albeit at different reactant concentrations [8,12,19–21]. This implies that the polymer matrix does not block Au NP formation, but it does affect particle sizes, which can be ascribed to diffusion-limited transport of both gold ions and the reducing agent. This suggests the size of Au NPs generated at a polymer surface by *in-situ* reduction and their distribution in depth relative to the interface can be controlled by choice of the reducing agent.

Alternative binding agents and surface functionalization chemistry were examined as means for confining gold-ion binding and

[1] This value is based on one-electron irreversible oxidation of citrate observed by cyclic voltametry [49] Evidence for two-electron decarboxylation to dicarboxyacetone has been obtained in studies of gold nanoparticles synthesized in solution [19,50] and may therefore be relevant to the present work. The corresponding reduction potential can be estimated as −0.35 V based on values for two-electron oxidative decarboxylation of malate (−0.330 V) and isocitrate (−0.375 V) at pH 7 [51].

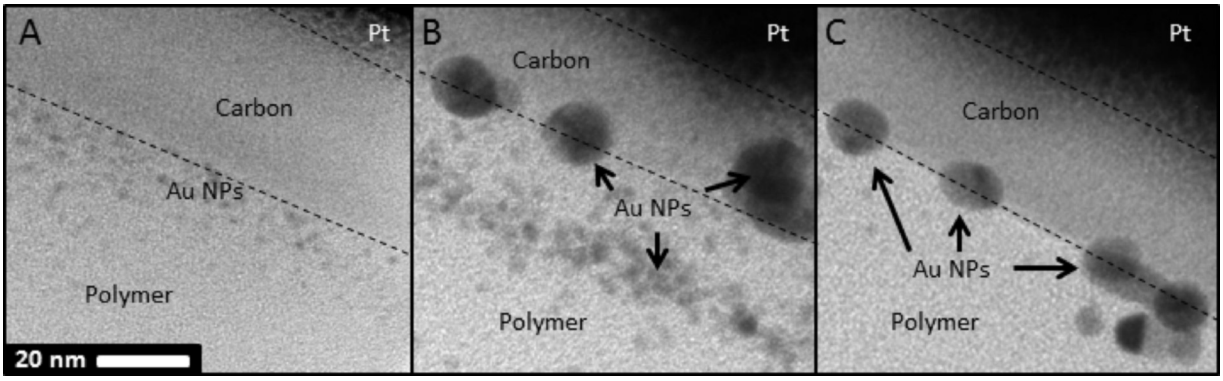

Fig. 5. TEM bright-field cross-sectional images of Au NP decorated films prepared using (A) $NaBH_4$, (B) sodium citrate, and (C) hydroquinone. The scale bar is applicable to all images. The dashed lines demarcate the approximate interfaces between the polymer, carbon, and Pt layers.

subsequent Au–NP formation to the polymer interface. Ethanol was replaced by water as the solvent for reacting amines with the polymer because water does not swell SU-8 [52–54], so it was expected to reduce transport of the binding agent into the polymer matrix. Additionally, the alternative binding agents AEP and TEPA were used in place of ED, on the assumption that their larger size would decrease their ability to penetrate into the polymer matrix. These experiments were performed with $NaBH_4$ as the reducing agent and were otherwise identical in all other ways to procedures described above.

When either aqueous AEP or TEPA was used for binding agent attachment, the Au NPs form in a single layer near the interface approximately one particle-width thick (compare Fig. 6A and B with Fig 5A). If the larger amines were able to penetrate into the polymer appreciably under aqueous condition and bind gold ions below the surface, or if gold ions could embed within the polymer matrix unbound by the amine, then small Au NPs should have been observed, as in Fig. 5A. The absence of Au NPs substantially below the interface supports the hypothesis that TEPA and AEP are unable to penetrate significantly into the polymer matrix and that these larger amines bind gold ions at the interface. Additionally, because the Au NPs that do form near the interface are comparable in size to those observed in Fig. 5A, it provides additional evidence that the size is largely determined by the strength of the reducing agent. This approach decouples the effect of the reducing agent on influencing size of the NPs and the depth at which they form. By using larger binding agents and functionalizing the surface in water, formation of Au NPs can be confined near the interface, whereas their size can be independently controlled through choice of reducing agent.

3.3. The polymer matrix as a reservoir for metal ions

From HAADF–STEM images of Au NPs like that in Fig. 4, we can calculate what the effective number of gold atoms is per *projected* unit surface area. It is instructive to compare this value to what the *maximum* coverage of gold ions at the interface could be prior to reduction, and to reflect on what this implies about the role of the polymer matrix during formation of Au NPs by *in situ* reduction.

Based on the number of Au NPs found per region, their average volume, and assuming gold atoms adopt a face-center-cubic packing within the NPs, the *projected* gold atom surface density across five different regions was found to be 10 to 13 atoms nm^{-2} with a mean surface density of 12 atoms nm^{-2}. Now let us calculate what the maximum gold-ion coverage could be at the interface prior to reduction. First, let us assume that gold ions bind to the interface as a monolayer of $AuCl_4^-$ units packed as tightly as possible-an hexagonally close-packed arrangement of square-planar $AuCl_4^-$ anions oriented with the coordination plane perpendicular to the surface. Based on the dimensions of the $AuCl_4^-$ anion observed for crystalline $KAuCl_4{\cdot}2H_2O$ [55], we can estimate that the gold-ion surface density could at most be 6 atoms nm^{-2} prior to reduction. Note

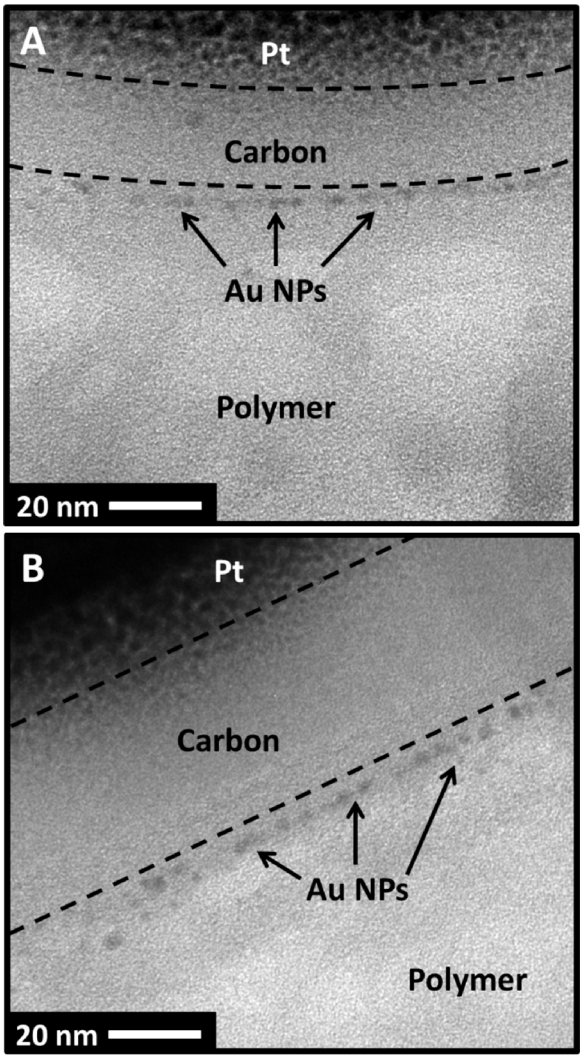

Fig. 6. TEM cross-sections of Au NPs created when the polymer is functionalized with the alternative binding agents (A) AEP and (B) TEPA in water. The scale bar applies to both images. The dashed lines demarcate the interface between the polymer and the layers of carbon and platinum used to prepare the sample cross section. Note that the NPs reside in a single band roughly the width of the particles themselves.

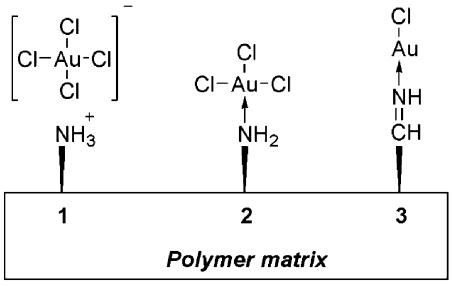

Fig. 7. Possible modes for chemisorption of gold ions at the amine-functionalized polymer surface, both at and below the interface.

that this represents an upper limit because the surface-packing arrangement assumed is even denser than that found for crystalline $KAuCl_4{\cdot}2H_2O$. Thus, HAADF–STEM images of the Au NP-decorated polymer film give a number of gold atoms observed per projected unit surface area that is twice as large as the number of gold atoms that could possibly bind at the interface under the densest arrangement possible.

The analysis above suggests that either the Au ions aggregate on the surface or they diffuse into the polymer matrix, so that the polymer functions as a reservoir for gold ions during *in-situ* reduction at or near the interface. Support for the former hypothesis is offered in Section 3.5, where AFM measurements of the films are discussed. Support for the latter hypothesis can be found from the cross-sectional images of the samples, like that in Fig. 5A, which show that most of the Au NPs produced by $NaBH_4$ reduction are not actually on the surface, but rather are buried within the polymer matrix at a depth as much as 20 nm below the interface. This in turn implies that both metal ions and the reducing agent can diffuse into the polymer matrix. It is well documented that solvents can swell cross-linked polymers, including SU-8 [52–54,56–58], and this effect can be used to chemically modify polymeric surfaces [59,60]. This provides support for the hypothesis that both the metal ion source and the reducing agent $NaBH_4$ appear to penetrate into the polymer matrix, leading to formation of Au NPs below the interface.

The observations described above suggest that *in-situ* reduction does not always occur solely at the interface of a polymeric surface. Other types of surface chemistry conducted at polymeric surfaces may likewise involve diffusion of species into the polymeric matrix, and the matrix itself may be equally or more important to the progress of such reactions as the solution medium at the interface.

3.4. XPS analysis of surface-bound gold

At least three bonding modes (Fig. 7) can be envisioned for chemisorption of gold ions onto an amine-functionalized polymer. These include neutral and charged Au(III) and Au(I) species. (1) Ion pairing of $AuCl_4^-$ with a protonated amine could form a charged Au(III) species. (2) The amine could displace a chloride ligand and eliminate HCl, forming a covalently bound neutral Au(III) species. And by analogy with the known reaction of $AuCl_4^-$ with alkylamines in solution [61], (3) the amine could partially reduce Au(III) to Au(I) with loss of HCl and formation of an Au(I)-imine complex. To identify the most likely bonding mode, XPS analysis was carried out for SU-8 films aminated with ED, AEP or TEPA, and then treated with $HAuCl_4$. These spectra were compared to XPS data in the literature for reference compounds containing Au(III), Au(I), and Au(0) species [42,62,63] Analysis of gold oxidation states via XPS is complicated by the fact that X-rays can induce reductive decomposition of Au(III) [62,63]. For this reason, XPS spectra were collected as a function of X-ray exposure time to obtain a time-dependent analysis of the Au oxidation state.

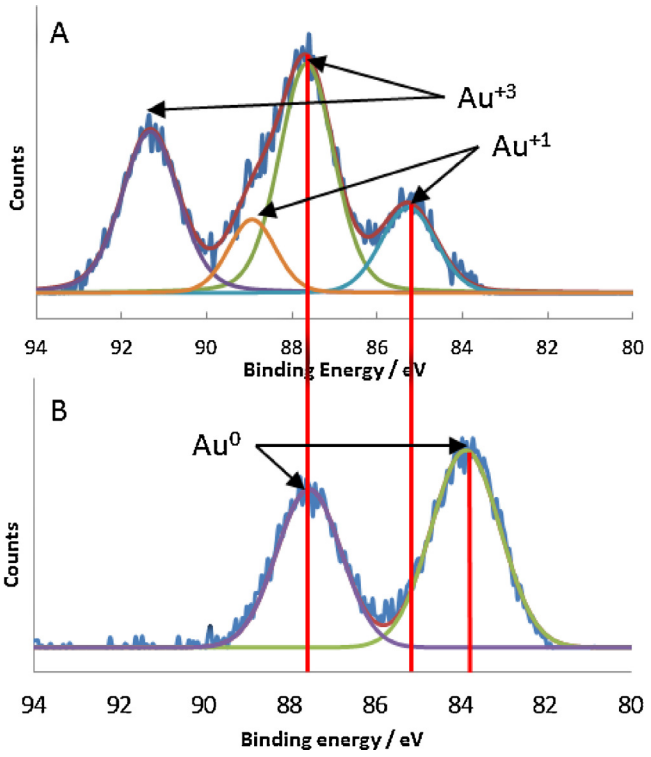

Fig. 8. XPS spectra of gold bound to SU-8 polymer films using ED (A) after treatment with $HAuCl_4$ and (B) after chemical reduction using $NaBH_4$ to form Au NPs. The experimental data (*blue curve*) were fit (*purple curve*) by summing one or more Gaussian-Lorentzian doublets (*remaining colors*), which correspond to oxidation states Au(0), Au(I), and Au(III). The red vertical lines indicate the locations of the $4f_{7/2}$ peaks for each oxidation state. Panel A is the first in a time-resolved sequence of XPS spectra that were recorded to assess how X-ray exposure affects the oxidation state of surface-bound gold. The time-resolved changes in the area of the Au(I) and Au(III) peaks are depicted in Fig. 9. (For interpretation of the references to color in this figure legend, the reader is referred to the web version of this article.)

Fig. 8A shows the first of a series of spectra obtained through time-resolved XPS analysis of an SU-8 polymer film that was aminated with ED then treated with $HAuCl_4$. The dominant features at 87.7 eV and 91.4 eV correspond to Au(III), whereas the weaker peak at 85.3 eV and the shoulder at 88.9 eV correspond to Au(I) [42,62,63]. The Au(III) peaks were found to diminish progressively

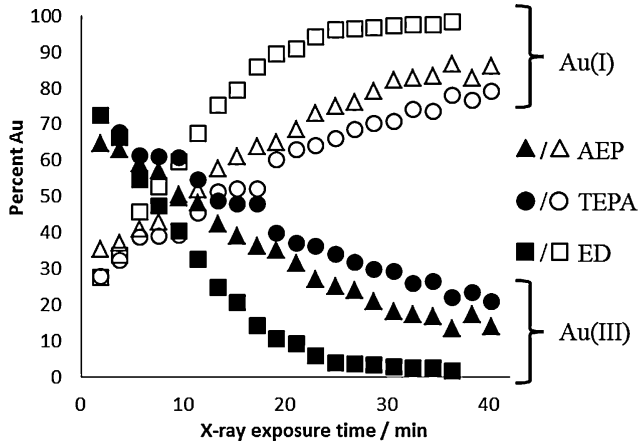

Fig. 9. Atomic percentage of Au(I) and Au(III) observed as a function of exposure time during XPS measurements of SU-8 polymer films bearing gold affixed using the binding agents ED, AEP, or TEPA. Hollow markers represent Au(I) and filled markers represent Au(III). These data were obtained from time resolved spectra, like that in Fig. 8A, by integrating the areas of the $4f_{7/2}$ peaks used to represent Au(I) and Au(III) in the best fit of each spectrum.

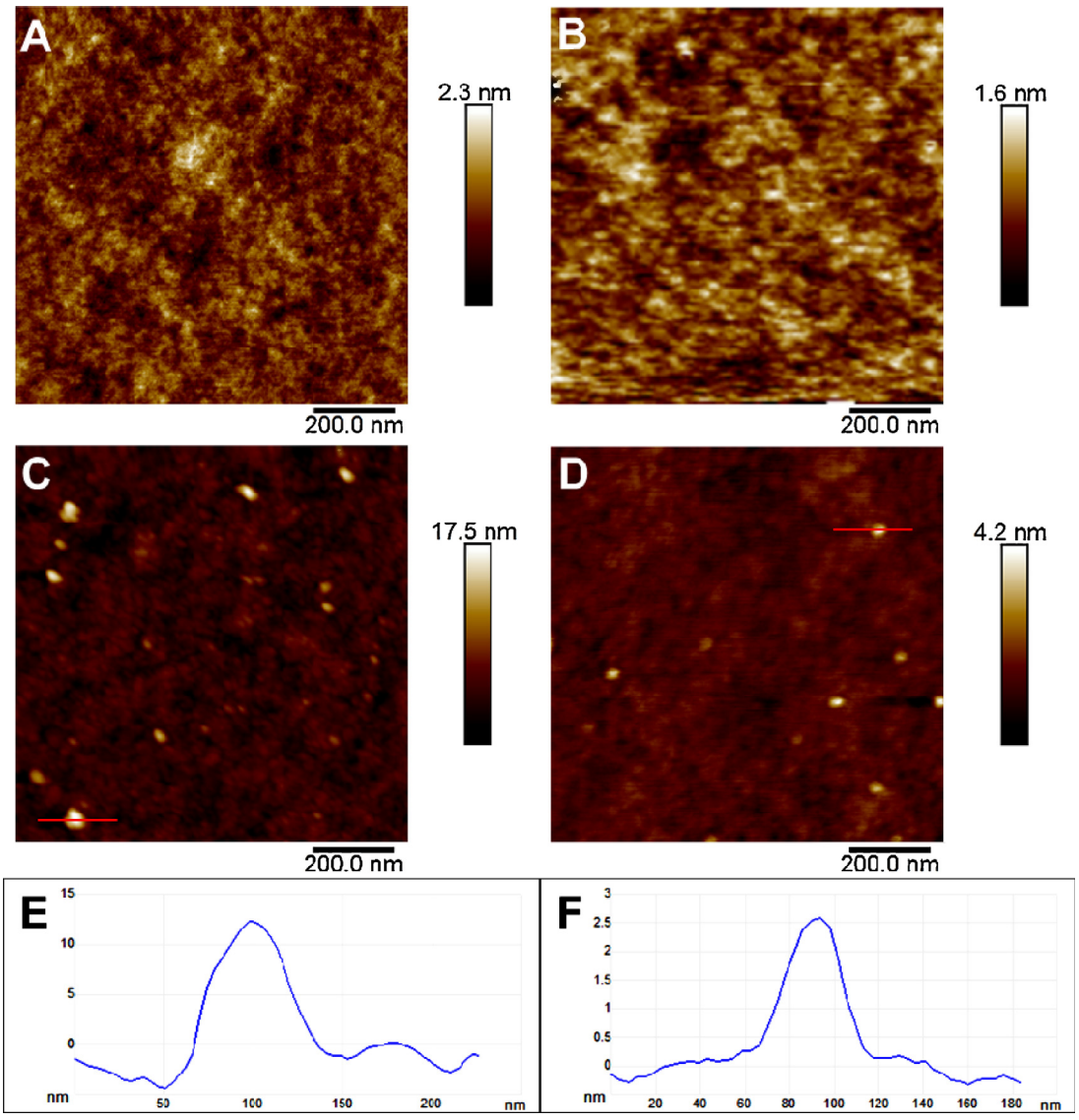

Fig. 10. (A–D) Surface topography of the SU-8 films at various stages in the Au–NP synthesis process as measured by AFM: (A) pristine polymeric film; (B) after treatment with ED; (C) after treatment with ED and $HAuCl_4$; (D) after treatment with ED and $HAuCl_4$ followed by reduction with $NaBH_4$. (E–F) Line scans of the features indicated by the red lines in (C) and (D), respectively.

with each subsequent scan, whereas the Au(I) peaks increase concomitantly. Similar behavior was observed for samples prepared using the binding agents AEP and TEPA. The areas of the $4f_{7/2}$ peaks were measured for each oxidation state and plotted versus time, as shown in Fig. 9, to quantify the atomic-percentage of gold in each oxidation state as a function of X-ray exposure time. After a period of less than 20 min, the amount of Au(III) on all of the aminated samples had been reduced to less than 50%, and less than 20% after a period of 40 min. These time scales are long compared to the 120 s required to obtain an individual spectrum, so each data point may be regarded as an instantaneous snapshot of the gold oxidation states present at the sample. It is interesting to note that the rate at which X-ray exposure decomposes Au(III) to Au(I) differs with the binding agents. X-ray induced decomposition was fastest for ED, which contains only primary amines, and slower for AEP and TEAP, which contain secondary and tertiary amines. This suggests that the binding group, depending upon its structure, can partially stabilize Au(III) against X-ray-induced decomposition.

These observations are similar to the findings of Buntine et al. [63] with some key differences. In their report, soft X-ray exposure of Au(III) supported on silicon produced Au(I), which decomposed further to Au(0) within *circa* 15 min, following first-order kinetics. The time constants found by Buntine et al. are shorter than that observed in the present work, perhaps because the synchrotron source they used provided high X-ray flux. But more intriguing is that under our conditions no Au(0) was observed, not even after 70 min of X-ray exposure. Au(0) was only detected when samples were subjected to chemical reduction, using $NaBH_4$, citrate, or hydroquinone. For example, Fig. 8B shows the XPS spectrum obtained for a sample having Au ions bound to the surface with ED then chemically reduced using $NaBH_4$. Only two peaks are observed. These are located at 87.6 eV and 83.9 eV and have integrated areas in a ratio of 3:4, as expected for the $4f_{5/2}$ and $4f_{7/2}$ peaks of Au(0) [42,62,63]. This shows that the NPs formed by chemical reduction consist of Au atoms in oxidation state zero.

Extrapolating the time-resolved data to the time-origin suggests that the gold ions bind primarily as Au(III), but approximately 20% binds as Au(I). The Au–Cl ratios were also examined, and were found for long exposure times to be nearly 1:1. This is consistent with the surface-bound gold evolving to the Au(I)-imine complex

shown in Fig. 7 (mode 3). It was not possible to distinguish whether Au(III) was present in the ionic or neutral complex form shown in Fig. 7 (modes 1 and 2). Au(0) was only found when samples were chemically reduced using $NaBH_4$, citrate, or hydroquinone, which resulted in formation of gold NPs as described above. It is noteworthy that secondary and tertiary amines have been reported to be capable of reducing $AuCl_4^-$ to Au(0) in solution, forming Au NPs [33,64–66], whereas primary amines cannot [65,66]. Yet no evidence for Au(0) was found-even when binding gold ions using agents like AEP and TEPA that contain secondary and tertiary amines-until the samples were forcibly reduced using $NaBH_4$, citrate, or hydroquinone.

3.5. AFM analysis of films

Results of the AFM measurements are shown in Fig. 10, for the example of films processed using ED as the binding agent. Pristine SU-8 films exhibit an RMS surface roughness much below 1 nm, typically between 0.2 and 0.3 nm. Treatment with ED, AEP, or TEPA increases the surface roughness slightly, to between 0.3 and 0.4 nm. Distinct features with height above 1 nm first appear upon treating the aminated films with Au(III). In the case of Au(III) bound with ED, the RMS roughness increases to 1.3 nm, and line-scans across the biggest features show maximum height excursions as large as 17 nm (Fig. 10E), although these are comparatively few in number. Such features are also visible on films having Au(III) bound with AEP and TEPA, but they are much smaller and more numerous, with RMS roughness of ~0.4 nm, and maximum height excursions of 6.2 and 4.8 nm, respectively. As no evidence was found by XPS for Au(0) prior to reduction, we conclude these features are most likely small aggregates of surface-bound Au(III) salt. These observations provide some evidence to support the second hypothesis introduced in Section 3.3, that the surface itself could bear clusters of Au(III) precursor that serve as reservoirs for gold atoms during reduction.

Distinct features larger than 1 nm remain present after the Au(III)-functionalized samples are treated with a reducing agent. Interestingly, the RMS roughness decreases substantially for ED-treated films, dropping to 0.3 nm, with maximum height excursions of 5.3 nm for treatment with $NaBH_4$ (Fig. 10D and F). This is consistent with the TEM cross-sectional measurements that show small Au NPs resulting upon reduction with a diameter of 5 nm or smaller. This implies that the reduction actually breaks up the larger salt-aggregates seen in Fig. 10C. Similarly sized Au NPs are observed for AEP- and TEPA-treated samples after reducing with $NaBH_4$. When ED/Au(III)-functionalized surfaces are treated with either citrate or hydroquinone, AFM measurements reveal distinct features having height greater than 5 nm, which suggests that nanoparticles have formed which are larger than those resulting from reduction with $NaBH_4$. These observations are all consistent with those obtained from the TEM cross-sectional measurements.

4. Conclusion

This work shows that synthesizing Au NPs at a cross-linked polymer surface by *in-situ* reduction of metal cations does not necessarily generate particles solely at the liquid-polymer interface. Reducing agents commonly used to synthesize NPs in solution, such as $NaBH_4$ and citrate, can generate particles within the cross-linked polymer SU-8 as much as 40 nm below the surface. In contrast, hydroquinone appears to generate NPs only at the interface. It is proposed that diffusion of the metal cation and the reducing agent through the polymer matrix affects the size of Au NPs formed and the depth at which they are generated, and that this can be controlled through the choice of reducing agent and the gold-ion binding agent. Conditions that restrict attachment of the binding agent at the interface likewise favor Au–NP generation on the surface, even when $NaBH_4$ is used as the reducing agent. NPs generated at the interface by citrate and hydroquinone are much larger than those generated below the surface. When the strong reducing agent $NaBH_4$ is reacted with Au ions bound at the interface, the rapid reaction favors nucleation over growth yielding only small NPs, all bound at or very near the interface. Particles generated by *in-situ* reduction with $NaBH_4$ on SU-8 are shown to be oblate spheroids.

These results suggest it may be possible to control synthesis of Au NPs below the interface of a polymer. This could be useful for several emerging applications in photonics. For example, it is well known that metal NPs can be used to achieve dramatic field enhancement of optical effects [67–69]. In the case of fluorescence, the overall emission enhancement is optimized at a certain distance from the NP, because absorption enhancement and NP-induced quenching are competing effects that exhibit different distance dependence [70]. As such, controlling the depth at which Au NPs are created below a surface by the method reported here may be useful for creating material systems with controlled optical enhancement that are not compromised by fluorescence quenching.

Acknowledgments

This work was supported by NSF CAREER grant DMR/CHE-0748712 and NSF grant CHE-0809821. CJK was supported at the University of Central Florida (UCF) by the Beckman Scholars Program. DJF was supported by NSF grant nos. 0525429 and 0806931. CNG was supported by an REU supplement to NSF grant no. 0748712. MAH was supported by a UCF SURF Scholarship. We thank Dr. Florencio E. Hernandez for helpful discussions concerning potential applications of this work, Dr. Andre Gesquiere and Mr. Ernie Gemeinhart of the UCF NanoScience Technology Center for assistance with the AFM measurements, and the reviewers for their many helpful comments.

References

[1] M. Khalid, I. Pala, N. Wasio, K. Bandyopadhyay, Functionalized surface as template for *in situ* generation of two-dimensional metal nanoparticle assembly, Colloids Surf., A 348 (2009) 263–269.
[2] Q. Zhang, J.-J. Xu, Y. Liu, H.-Y. Chen, *In-situ* synthesis of poly(dimethylsiloxane)–gold nanoparticles composite films and its application in microfluidic systems, Lab Chip 8 (2008) 352–357.
[3] W. Zhao, S.-X. Sun, J.-J. Xu, H.-Y. Chen, X.-J. Cao, X.-H. Guan, Electrochemical identification of the property of peripheral nerve fiber based on a biocompatible polymer film via in situ incorporating gold nanoparticles, Anal. Chem. 80 (2008) 3769–3776.
[4] H. He, W. Cai, Y. Lin, B. Chen, Surface decoration of ZnO nanorod arrays by electrophoresis in the Au colloidal solution prepared by laser ablation in water, Langmuir 26 (2010) 8925–8932.
[5] D. Kisailus, M. Najarian, J.C. Weaver, D.E. Morse, Functionalized gold nanoparticles mimic catalytic activity of a polysiloxane-synthesizing enzyme, Adv. Mater. 17 (2005) 1234–1239.
[6] M.A. Rahman, J.I. Son, M.-S. Won, Y.-B. Shim, Gold nanoparticles doped conducting polymer nanorod electrodes: ferrocene catalyzed aptamer-based thrombin immunosensor, Anal. Chem. 81 (2009) 6604–6611.
[7] A.C. Henry, R.L. McCarley, Selective deposition of metals on plastics used in the construction of microanalytical devices: photo-directed formation of metal features on PMMA, J. Phys. Chem. B 105 (2001) 8755–8761.
[8] W.-C. Li, S.-E. Park, J. Kim, S.-W. Lee, Self-assembled two-dimensional array of gold nanoparticles with different size for the sensing application, Jpn. J. Appl. Phys. 48 (2009) 06FF14.
[9] B. Tian, P. Xie, T.J. Kempa, D.C. Bell, C.M. Lieber, Single-crystalline kinked semiconductor nanowire superstructures, Nature Nanotechnol. 4 (2009) 824–829.
[10] A. Corma, H. Garcia, Supported gold nanoparticles as catalysts for organic reactions, Chem. Soc. Rev. 37 (2008) 2096–2126.
[11] F. Mancin, L.J. Prins, P. Scrimin, Catalysis on gold-nanoparticle-passivating monolayers, Curr. Opin. Colloid Interface Sci. 18 (2013) 61–69.
[12] K.C. Grabar, R.G. Freeman, M.B. Hommer, M.J. Natan, Preparation and characterization of Au colloid monolayers, Anal. Chem. 67 (1995) 735–743.
[13] T.S. Sreeprasad, T. Pradeep, Reversible assembly and disassembly of gold nanorods induced by EDTA and its application in SERS tuning, Langmuir 27 (2011) 3381–3390.

[14] B. Guo, S. Zhao, G. Han, L. Zhang, Continuous thin gold films electroless deposited on fibrous mats of polyacrylonitrile and their electrocatalytic activity towards the oxidation of methanol, Electrochim. Acta 53 (2008) 5174–5179.
[15] S. Kreitz, C. Penache, M. Thomas, C.P. Klages, Patterned DBD treatment for area-selective metallization of polymers-plasma printing, Surf. Coat. Technol. 200 (2005) 676–679.
[16] J. Qiu, M. Guo, Y. Feng, X. Wang, Electrochemical deposition of branched hierarchical ZnO nanowire arrays and its photoelectrochemical properties, Electrochim. Acta 56 (2011) 5776–5782.
[17] J.H.G. Ng, M.P.Y. Desmulliez, K.A. Prior, D.P. Hand, Ultra-violet direct patterning of metal on polyimide, Micro Nano Lett. 3 (2008) 82–89.
[18] S.-J. Huo, X.-K. Xue, Q.-X. Li, S.-F. Xu, W.-B. Cai, Seeded-growth approach to fabrication of silver nanoparticle films on silicon for electrochemical ATR surface-enhanced IR absorption spectroscopy, J. Phys. Chem. B 110 (2006) 25721–25728.
[19] J. Turkevich, P.C. Stevenson, J. Hillier, The formation of colloidal gold, J. Phys. Chem. 57 (1953) 670–673.
[20] M.-C. Daniel, D. Astruc, Gold nanoparticles: assembly, supramolecular chemistry, quantum-size-related properties, and applications toward biology, catalysis, and nanotechnology, Chem. Rev. 104 (2004) 293–346.
[21] I. Ojea-Jimenez, F.M. Romero, N.G. Bastús, V. Puntes, Small gold nanoparticles synthesized with sodium citrate and heavy water: insights into the reaction mechanism, J. Phys. Chem. C 114 (2010) 1800–1804.
[22] R.G. DiScipio, Preparation of colloidal gold particles of various sizes using sodium borohydride and sodium cyanoborohydride, Anal. Biochem. 236 (1996) 168–170.
[23] C. Gómez-Lahoz, F. García-Herruzo, J.M. Rodríguez-Maroto, J.J. Rodríguez, Copper removal from water by chemical reduction with sodium borohydride, Sep. Sci. Technol. 27 (1992) 1449–1468.
[24] T. Ishida, K. Kuroda, N. Kinoshita, W. Minagawa, M. Haruta, Direct deposition of gold nanoparticles onto polymer beads and glucose oxidation with H_2O_2, J. Colloid Interface Sci. 323 (2008) 105–111.
[25] A. Tal, Y.-S. Chen, H.E. Williams, R.C. Rumpf, S.M. Kuebler, Fabrication and characterization of three-dimensional copper metallodielectric photonic crystals, Opt. Express 15 (2007) 18283–18293.
[26] X. Chen, D.Y. Zhao, L.Z. Zhao, Y.L. An, R.J. Ma, L.Q. Shi, Q.J. He, L. Chen, Optic and catalytic properties of gold nanoparticles tuned by homopolymers, Sci. China, Ser. B—Chem. 52 (2009) 1372–1381.
[27] S.-N. Li, X.-L. Yang, W.-Q. Huang, Preparation of polymer microspheres with pyridyl group and their stabliized gold metallic colloids, Chin. J. Polym. Sci. 25 (2007) 555–563.
[28] Y. Liu, S.Z.D. Cheng, X. Wen, J. Hu, Preparing and stabilizing colloidal nanoparticles with a helical synthetic polymer, Langmuir 18 (2002) 10500–10502.
[29] Z. Peng, E. Wang, S. Dong, Incorporation of surface-derivatized gold nanoparticles into electrochemically generated polymer films, Electrochem. Commun. 4 (2002) 210–213.
[30] L. Zhong, T. Jiao, M. Liu, Synthesis and assembly of gold nanoparticles in organized molecular films of gemini amphiphiles, Langmuir 24 (2008) 11677–11683.
[31] Y. Xu, Q. Cao, F. Svec, J.M.J. Fréchet, Porous polymer monolithic column with surface-bound gold nanoparticles for the capture and separation of cysteine-containing peptides, Anal. Chem. 82 (2010) 3352–3358.
[32] F.Y. Pong, M. Lee, J.R. Bell, N.T. Flynn, Thermoresponsive behavior of poly(*n*-isopropylacrylamide) hydrogels containing gold nanostructures, Langmuir 22 (2006) 3851–3857.
[33] J. Newman, G. Blanchard, Formation and encapsulation of gold nanoparticles using a polymeric amine reducing agent, J. Nanopart. Res. 9 (2007) 861–868.
[34] A. Mata, E.J. Kim, C.A. Boehm, A.J. Fleischman, G.F. Muschler, S. Roy, A three-dimensional scaffold with precise micro-architecture and surface micro-textures, Biomaterials 30 (2009) 4610–4617.
[35] J.-S. Yeo, H. Lewis, N. Meyer, Nanofabrication with laser holographic lithograpy for nanophotonic structures, J. Laser Micro/Nanoeng. 2 (2007) 31–35.
[36] R. Yang, B.-R. Lu, J. Xue, Z.-K. Shen, Z.-C. Xu, E. Huq, X.-P. Qu, Y. Chen, R. Liu, Nanoimprint lithography for optic fluidics with phase gratings for environmental monitoring application, Microelectron. Eng. 87 (2010) 824–826.
[37] Y.-S. Chen, A. Tal, S.M. Kuebler, Route to three-dimensional metallized microstructures using cross-linkable epoxide SU-8, Chem. Mater. 19 (2007) 3858–3860.
[38] R.A. Farrer, C.N. LaFratta, L. Li, J. Praino, M.J. Naughton, B.E.A. Saleh, M.C. Teich, J.T. Fourkas, Selective functionalization of 3-D polymer microstructures, J. Am. Chem. Soc. 128 (2006) 1796–1797.
[39] G. Danscher, Localization of gold in biological tissue: a photochemical method for light and electronmicroscopy, Histochemistry 71 (1981) 81–88.
[40] D. Briggs, Surface Analysis of Polymers by XPS and Static SIMS, Cambridge University Press, Cambridge, 1998.
[41] B. Bêche, P. Papet, D. Debarnot, E. Gaviot, J. Zyss, F. Poncin-Epaillard, Fluorine plasma treatment on SU-8 polymer for integrated optics, Opt. Commun. 246 (2005) 25–28.
[42] C.D. Wagner, G.E. Muilenberg, Handbook of X-Ray Photoelectron Spectroscopy: A Reference Book of Standard Data for Use in X-ray Photoelectron Spectroscopy, Perkin-Elmer Corp, 1979.
[43] A. Sirajuddin, A.A.J. Mechler, A. Torriero, C.-Y. Nafady, A.M. Lee, A.P. Bond, S.K. O'Mullane, Bhargava, The formation of gold nanoparticles using hydroquinone as a reducing agent through a localized pH change upon addition of NaOH to a solution of $HAuCl_4$, Colloids Surf., A 370 (2010) 35–41.
[44] R. Shankar, V. Shahi, U. Sahoo, Comparative study of linear poly(alkylarylsilane)s as reducing agents toward Ag(I) and Pd(II) ions-synthesis of polymer-metal nanocomposites with variable size domains of metal nanoparticles, Chem. Mater. 22 (2010) 1367–1375.
[45] A. Troupis, T. Triantis, A. Hiskia, E. Papaconstantinou, Rate-redox-controlled size-selective synthesis of silver nanoparticles using polyoxometalates, Eur. J. Inorg. Chem. 2008 (2008) 5579–5586.
[46] M.T. Reetz, M. Maase, Redox-controlled size-selective fabrication of nanostructured transition metal colloids, Adv. Mater. 11 (1999) 773–777.
[47] N.G. Gaylord, Reduction with Complex Metal Hydrides, Interscience Publishers, New York, NY, 1956.
[48] R. Chang, Physical Chemistry for the Biosciences, University Science Books, Mill Valley, CA, 2005.
[49] O. Berkh, L. Burstein, Y. Shacham-Diamand, E. Gileadic, The chemical and electrochemical activity of citrate on Pt electrodes, J. Electrochem. Soc. 158 (2011) F85–F91.
[50] S. Kumar, K.S. Gandhi, R. Kumar, Modeling of formation of gold nanoparticles by citrate method, Ind. Eng. Chem. Res. 46 (2007) 3128–3136.
[51] C. Long, Biochemists' Handbook, D. van Norstrand Co., Inc., Princeton, 1968.
[52] K. Wouters, R. Puers, Accurate measurement of the steady-state swelling behavior of SU-8 negative photo resist, Procedia Chem. 1 (2009) 60–63.
[53] K. Wouters, R. Puers, Diffusing and swelling in SU-8: insight in material properties and processing, J. Micromech. Microeng. 20 (2010) 095013.
[54] C. Liu, Y. Liu, M. Sokuler, D. Fell, S. Keller, A. Boisen, H.-J. Butt, G.K. Auernhammer, E. Bonaccurso, Diffusion of water into SU-8 microcantilevers, Phys. Chem. Chem. Phys. 12 (2010) 10577–10583.
[55] F. Theobald, H. Omrani, Structure du tetrachloroaurate(III) de potassium dihydrate, Acta Crystallogr. B 36 (1980) 2932–2935.
[56] Y. Wang, W. Monch, B. Aatz, H. Zappe, Tunable photonic crystals on a freestanding polymer membrane, J. Micromech. Microeng. 20 (2010) 015003.
[57] G.C. Hill, R. Melamud, F.E. Declercq, A.A. Davenport, I.H. Chan, P.G. Hartwell, B.L. Pruitt, SU-8 MEMS Fabry–Perot pressure sensor, Sens. Actuators, A: Phys. 138 (2007) 52–62.
[58] J. Hsieh, C.J. Weng, H.L. Yin, H.H. Lin, H.Y. Chou, Realization and characterization of SU-8 micro cylindrical lenses for in-plane micro optical systems, Microsyst. Technol. 11 (2005) 429–437.
[59] H.-N. Kim, J.-H. Kang, W.-M. Jin, J.H. Moon, Surface modification of 2D/3D SU-8 patterns with a swelling-deswelling method, Soft Matter 7 (2011) 2989–2993.
[60] J. Ford, S.R. Marder, S. Yang, Growing "nanofruit" textures on photo-crosslinked SU-8 surfaces through layer-by-layer grafting of hyperbranched poly(ethyleneimine), Chem. Mater. 21 (2009) 476–483.
[61] Y. Nagel, W. Beck, Reaktionen von Tetrachloroaurat mit verschiedenen Aminen, Z. Anorg. Allg. Chem. 529 (1985) 57–60.
[62] F. Karadas, G. Ertas, E. Ozkaraoglu, S. Suzer, X-ray-induced production of gold nanoparticles on a SiO_2/Si system and in a poly(methyl methacrylate) matrix, Langmuir 21 (2005) 437–442.
[63] Y.-Y. Fong, B.R. Visser, J.R. Gascooke, B.C.C. Cowie, L. Thomsen, G.F. Metha, M.A. Buntine, H.H. Harris, Photoreduction kinetics of sodium tetrachloroaurate under synchrotron soft X-ray exposure, Langmuir 27 (2011) 8099–8104.
[64] M. Aslam, L. Fu, M. Su, K. Vijayamohanan, V.P. Dravid, Novel one-step synthesis of amine-stabilized aqueous colloidal gold nanoparticles, J. Mater. Chem. 14 (2004) 1795–1797.
[65] J.D.S. Newman, G.J. Blanchard, Formation of gold nanoparticles using amine reducing agents, Langmuir 22 (2006) 5882–5887.
[66] M.J. Richardson, J.H. Johnston, T. Borrmann, Monomeric and polymeric amines as dual reductants/stabilisers for the synthesis of gold nanocrystals: a mechanistic study, Eur. J. Inorg. Chem. 2006 (2006) 2618–2623.
[67] P.K. Jain, X. Huang, I.H. El-Sayed, M.A. El-Sayed, Review of some interesting surface plasmon resonance-enhanced properties of noble metal nanoparticles and their applications to biosystems, Plasmonics 2 (2007) 107–118.
[68] S. Zou, G.C. Schatz, Combining micron-size glass spheres with silver nanoparticles to produce extraordinary field enhancements for surface-enhanced raman scattering applications, Isr. J. Chem. 46 (2006) 293–297.
[69] H. Mishra, Y. Zhang, C.D. Geddes, Metal enhanced fluorescence of the fluorescent brightening agent Tinopal-CBX near silver island film, Dyes Pigm. 91 (2011) 225–230.
[70] S. Eustis, M.A. El-Sayed, Why gold nanoparticles are more precious than pretty gold: noble metal surface plasmon resonance and its enhancement of the radiative and nonradiative properties of nanocrystals of different shapes, Chem. Soc. Rev. 35 (2006) 209–217.